AIP | Applied Physics Letters

Electrically tunable terahertz quantum cascade lasers based on a two-sections interdigitated distributed feedback cavity

Dana Turčinková, Maria Ines Amanti, Giacomo Scalari, Mattias Beck, and Jérôme Faist

Citation: Applied Physics Letters **106**, 131107 (2015); doi: 10.1063/1.4916653
View online: http://dx.doi.org/10.1063/1.4916653
View Table of Contents: http://scitation.aip.org/content/aip/journal/apl/106/13?ver=pdfcov
Published by the AIP Publishing

Electrically tunable terahertz quantum cascade lasers based on a two-sections interdigitated distributed feedback cavity

Dana Turčinková,[1] Maria Ines Amanti,[1,2] Giacomo Scalari,[1] Mattias Beck,[1] and Jérôme Faist[1]
[1]*ETH Zurich, Institute for Quantum Electronics, Auguste-Piccard-Hof 1, 8093 Zurich, Switzerland*
[2]*Univ. Paris Diderot, Lab. Matererk iaux et Phenomenes Quantiques, F-75205 Paris, France*

(Received 26 January 2015; accepted 20 March 2015; published online 2 April 2015)

The continuous electrical tuning of a single-mode terahertz quantum cascade laser operating at a frequency of 3 THz is demonstrated. The devices are based on a two-section interdigitated third-order distributed feedback cavity. The lasers can be tuned of about 4 GHz at a constant optical output power of 0.7 mW with a good far-field pattern. © *2015 AIP Publishing LLC*.
[http://dx.doi.org/10.1063/1.4916653]

The terahertz quantum cascade laser (THz QCL) is an attractive light source for many scientific and commercial applications.[1–3] In many spectroscopy applications, such as, for example, the investigation of molecular lines in radio astronomy where a well defined molecular transition is investigated,[4,5] manufacturing devices emitting at the exact desired wavelength is challenging given the limits in the accuracy of the lithography and the uncertainties in the material constants. This concern, as well as the fact that many spectroscopy techniques require sweeping the frequency of the device across the molecular line, makes frequency tunability a very desired property of such devices.

Several tuning methods concerning THz QCLs have been realized, e.g., by temperature,[6] cavity pulling,[7,8] material condensation,[9,10] external cavity,[11] MEMS (microelectromechanical system),[12] use of coupled cavities,[13] or by a three-terminal configuration.[14] Methods relying strictly on a modification of the laser injection currents[6–8,14] are often preferred, thanks to their simplicity, speed, compactness, and flexibility. As compared to the mid-infrared QCLs[15] where temperature tuning is the preferred tuning mechanism, however, the latter is very inefficient for THz operating below 50 K because the refractive index remains essentially constant. In contrast, cavity pulling is much stronger in the THz than in the mid-infrared because of the very tightly confined cavities used and the larger values of the refractive index change accompanying the gain.

For this reason, tuning based on a cavity pulling effect, and where the change of refractive index is induced by the Stark shift of the laser transition, is a very attractive mechanism because it is essentially instantaneous and relies purely on an electrical drive mechanism with no moving parts. However, in lasers based on a single biased section, the frequency tuning is always accompanied by a change in output power. Furthermore, in high performance devices with very large ratios between the upper and lower state lifetimes, the voltage essentially clamps to a constant value at threshold, reducing significantly the tuning. In mid-infrared devices based on a photon-assisted tunneling transition, this problem is very acute. Strong tunability was nevertheless achieved by using a two-section device.[16] In this work, as shown schematically in Fig. 1, we investigate two-section THz lasers where, in contrast to,[16] single mode is achieved using a third-order distributed feedback (DFB) structure[17] and where an interdigitated electrode scheme[18] is implemented. In such a multi-terminal device, the clamping of the gain to the threshold value, responsible for the clamping of the voltage, is replaced by a global condition gain equal losses

$$G_{tot} = G_1 + G_2 = \Gamma_1 g_{c1} J_1 + \Gamma_2 g_{c2} J_2 = \alpha_{tot},$$

where Γ is the overlap factor of the optical mode and the gain medium, J is the current density, and g_c is the differential gain of the two stacks at the laser wavelength. While the total gain G_{tot} must still remain constant, the gain in each section can be adjusted independently.

As shown schematically in Figs. 1(a) and 1(b) and in a scanning electron micrograph of the device in Fig. 1(c), the structure is based on double metal waveguide and it is shaped

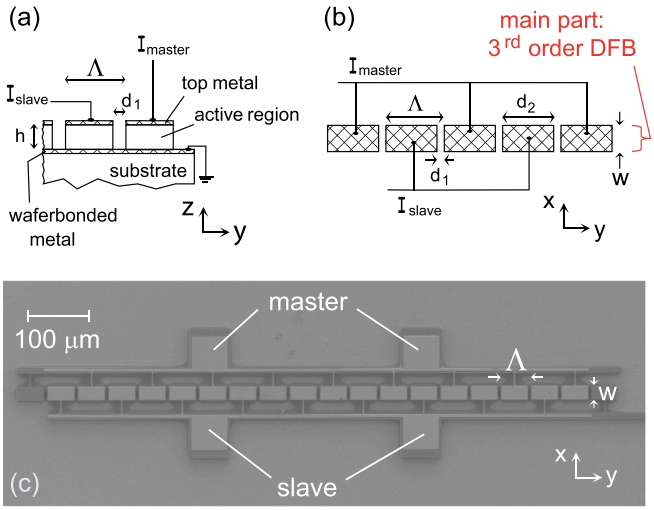

FIG. 1. Schematic drawing of the device (a) side and (b) top views. The two sections (master and slave) are independently pumped with electrical currents I_{master} and I_{slave}. The structure has the following parameters: height $h = 12\,\mu$m, width $w = 21\,\mu$m, period $\Lambda = 51.3\,\mu$m, length of one block $d_2 = 45.4\,\mu$m, and distance between blocks $d_1 = 5.9\,\mu$m. (c) Scanning electron micrograph of a final device. The devices include: the main part consisting of the interdigitated distributed feedback cavity, thin feeding fins bringing current to the blocks, and two thicker feeding lines connecting fins belonging to the appropriate sections which are equipped with two bonding pads.

into an interdigitated third-order distributed feedback cavity.[17] Such a cavity is well suited for frequency and far-field control of THz QCLs with small or even sub-wavelength waveguide transverse dimensions. Absorbing boundary conditions are employed[19] in order to prevent lasing action from feeding lines and bonding pads.

The tuning mechanism of the laser system is explained schematically in Figs. 2(a) and 2(b). Assume that the two sections, refereed here somewhat arbitrarily as "master" and "slave," are biased differently such that the slave section is pumped with a higher electrical current than the master section. As shown schematically in Fig. 2(b), let us also assume for simplicity that the laser mode is initially resonant with the peak gain of the master section. Due to the Stark shift in the slave section, the refractive index change due to the gain is negative in the slave section and zero in the master section. As a result, the current, resonant gain peak position, and refractive index will have the profiles along the cavity shown schematically in Fig. 2(a). As a result, the effective index of the DFB lasing mode n_{eff} will decrease with increasing current difference between the two sections and the laser wavelength, determined by the Bragg diffraction condition

$$\lambda_b = (2/3)\, n_{eff} \Lambda,$$

will decrease concomitantly. Note that the argument holds similarly for modes slightly detuned from the peak gain.

The optimal parameters of the distributed feedback cavity were found by performing finite element three-dimensional eigenfrequency simulations using a commercial software (Comsol Multiphysics).[20] The active region is based on a four-quantum-wells design with resonant phonon extraction[21] and employs GaAs/$Al_{0.15}Ga_{0.85}As$ material system grown by molecular beam epitaxy. The devices were processed into double-metal waveguides and the structure was defined by a deep dry etching down to the waferbonded metal, as shown in Fig. 1(a). The measurements were performed in pulsed operation in order to prevent failure of the feeding fins, at a heat sink temperature of 10 K. Note, however, that some devices not suitable for tuning because they exhibited broken feeding fins were nevertheless operated in c.w. mode. The light was detected with a pyroelectric detector (Gentec) calibrated by an absolute power meter (Thomas Keating) without any additional collection optics. The spectra were characteristized by a commercial Fourier-transform-infrared spectrometer (Bruker Vertex) equipped with a DTGS pyroelectric detector and a Mylar beamsplitter. The measurements were limited by a resolution of 0.075 cm^{-1}. The far-field beam patterns were obtained with a pyroelectric detector rotating around the sample. Two schemes of electrical pumping were employed. In the homogeneous pumping scheme, both sections are pumped equally while in the heterogeneous pumping scheme, the current in the master section is stepped progressively, while the slave section is continuously swept in current.

Fig. 3 illustrates the characteristics of a representative device obtained in the homogeneous pumping scheme. The device lases for an applied current per section between 85 mA and 150 mA, dissipates less than 5 W of electrical power and provides up to 1.4 mW peak optical power, corresponding to a slope efficiency of 30 mW/A. Furthermore, it emits over the whole dynamical range a single mode at a frequency of ~3.05 THz, in good agreement with the simulations. The spectral emission can be electrically tuned over a range of 5 GHz. A single lobed far-field pattern characteristic for the third-order mode[17,22] was observed.

In the heterogeneous pumping scheme, the devices demonstrated a single mode and single lobed emission too. No significant changes were observed in the far-field as a function of the different injection levels in the master and slave sections. This result is expected as the envelope of the electric field distribution, which is fixed by the absorbing boundary conditions and the grating periodicity, mainly determines the far-field beam pattern. Fig. 4 shows the emission frequencies (b) and the light intensities (a) as a function of master and slave currents; the color plot displays only points where the laser is above threshold.

Laser action is only achieved when pumping both sections, and the section with the lowest current must still have a current I > 72 mA. As a result, lasing can be switched on

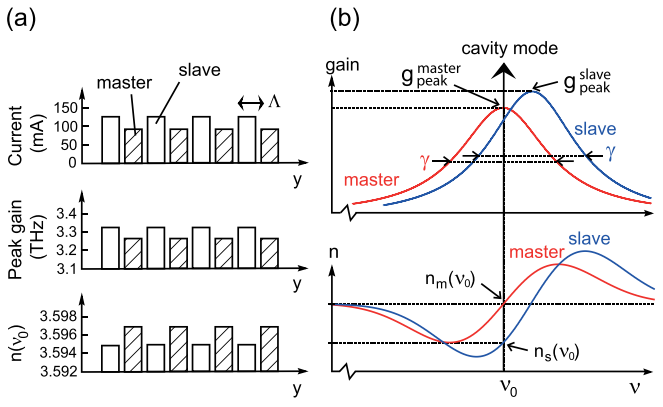

FIG. 2. Schematic explanation of operational principle of the laser system in a general case. (a) Simplified example of the values of the applied currents, frequencies of the peak gain, and the real part of the refractive index. (b) Gain distribution of the master and slave parts and the related index dispersion. ν_0 indicates the resonant frequency of a third-order mode of the passive cavity.

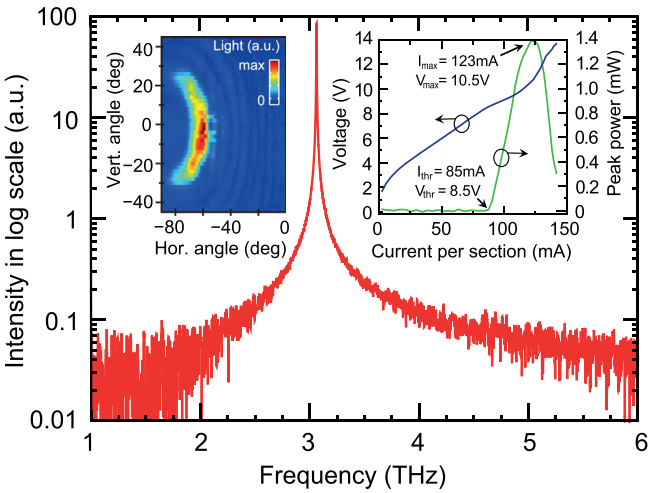

FIG. 3. Characteristics of a representative device measured in the homogeneous pumping scheme. Main: optical spectrum, inset left: corresponding far-field beam pattern, and inset right: voltage and light versus current per section.

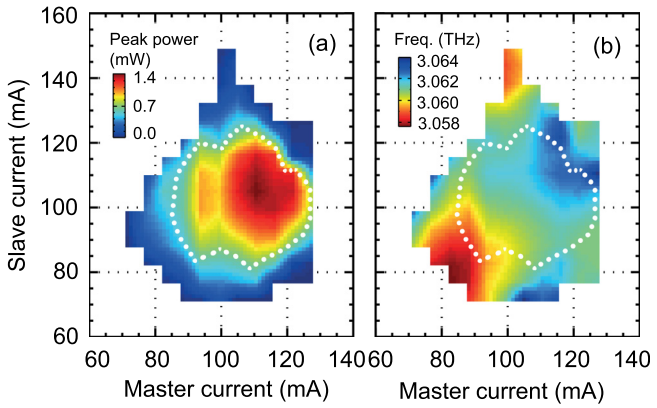

FIG. 4. (a) Optical output power and (b) frequency of the laser mode as a function of the master and slave currents. The white dotted line indicates the constant power of 0.7 mW.

and off by the electrical modulation of only one section. The single mode spectrum can be tuned over a total range of 7.5 GHz, larger than the value (5 GHz) obtained in the homogeneous pumping scheme. In addition, the device is able to tune with a fixed value of the optical power. As an example, a continuous tuning over a frequency range of 4 GHz is achieved for a fixed value of the optical output power of 0.7 mW. As expected from the discussion of the tuning mechanism, taking, for example, as a reference the symmetric pumping point (90 mA and 90 mA), the laser is observed to blue tune as the two currents are made more dissymmetric.

In Fig. 4, the optical output powers were calibrated by comparing the relative intensities to the maximum value obtained in the homogeneous measurements. The light-current characteristic of the device shown in Fig. 3 corresponds to the diagonal of the 2D plot shown in Fig. 4; the slight difference (6%) in the actual current values is attributed to differences in calibrations of the two current probes used in the measurement. The change in emission frequency $\Delta\nu$ is reported as a function of slave current for various master currents in Fig. 5(a). When $80 < I_S < 100$ mA, tuning with a positive slope is observed, as expected from our simple model. In contrast, for a slave current of $I_S \lesssim 80$ mA or

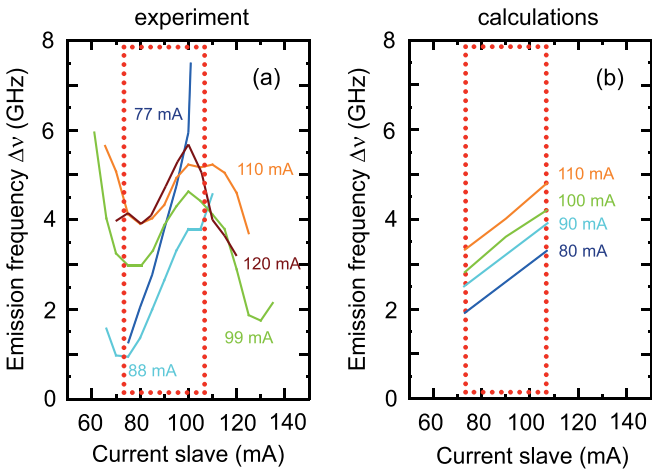

FIG. 5. Measured (a) and calculated (b) relative emission frequency $\Delta\nu = \nu_0 - \nu_{min}$ of the third-order DFB mode as a function of the slave current. Dependences for several representative master currents are indicated.

$I_S \gtrsim 100$ mA, the injector of the slave laser is not aligned with the upper state and a more complicated tuning behavior, with the opposite slope, is observed.

The measured tuning, in regime of resonant injection in the upper state (i.e., when $80 < I_S < 100$ mA), was compared with calculations based on transfer matrix method. In this one-dimensional model, the distributed feedback cavity was represented by periodically alternating layers of vacuum and the active material. The "effective" refractive index used in this simple model was fitted from a commercial three-dimensional full wave model of the whole cavity.[20] Furthermore, it was checked that a good agreement was obtained for the width of the photonic bandgap between the 1D and 3D models. The gain profile was assumed to be described by a simple Lorentzian distribution with a broadening of $\gamma = 1.5$ meV.[23] The Stark shift of the employed active material was determined from electroluminescence measurements on a non-lasing mesa. The tuning was found to be ~33 GHz/(kV/cm), which corresponds approximately to a shift of 100 GHz for our current range. A linear dependence of voltage and gain on current were assumed. In our model, the outcoupling loss of 7 cm^{-1} of our third-order grating was added and estimated using the three-dimensional electromagnetic solver.[20] Using this model, the calculated relative tuning of the resonant mode of the one dimensional cavity as a function of the slave current is shown in Fig. 5(b). A total tuning range of ~3 GHz with a positive tuning slope is obtained, in good agreement with the experimental results displayed in Fig. 5(a).

In conclusion, we demonstrated a DFB laser that allows a continuous tuning of a single mode emission at a constant output power with good far-field characteristics and optical powers. The tuning range achieved in the two-section configuration is larger than the one achieved using the standard one-section configuration. In particular, a frequency tuning of 4 GHz at constant optical power could be achieved. The tuning range is expected to improve by using another active region design with a higher gain or stronger Stark effect.

This work was supported by ETH Zurich with the FIRST cleanroom facility and by the Swiss National Science Foundation as well as a grant from the SFB 956 of the DFG. The author DT would like to thank Ralf Flueckiger for his advice regarding photolithography.

[1]J. Faist, F. Capasso, D. Sivco, C. Sirtori, A. Hutchinson, and A. Cho, Science **264**, 553 (1994).
[2]R. Köhler, A. Tredicucci, F. Beltram, H. Beere, E. Linfield, A. Davies, D. Ritchied, R. Iotti, and F. Rossi, Nature **417**, 156 (2002).
[3]M. Tonouchi, Nat. Photonics **1**, 97 (2007).
[4]T. G. Phillips and J. Keene, Proc. IEEE **80**(11), 1662 (1992).
[5]H. W. Huebers, IEEE J. Sel. Topi. Quantum Electron. **14**(2), 378 (2008).
[6]S. Kumar, B. S. Williams, Q. Qin, A. W. M. Lee, Q. Hu, and J. L. Reno, Opt. Express **15**(1), 113 (2007).
[7]L. A. Dunbar, R. Houdre, G. Scalari, L. Sirigu, M. Giovannini, and J. Faist, Appl. Phys. Lett. **90**, 141114 (2007).
[8]H. Zhang, G. Scalari, J. M. Faist, L. A. Dunbar, and R. Houdré, J. Appl. Phys. **108**(9), 093104 (2010).
[9]A. Benz, C. Deutsch, M. Brandstetter, A. M. Andrews, P. Klang, H. Detz, W. Schrenk, G. Strasser, and K. Unterrainer, Sensors **11**, 6003 (2011).

[10]D. Turcinkova, M. I. Amanti, F. Castellano, M. Beck, and J. Faist, Appl. Phys. Lett. **102**, 181113 (2013).
[11]A. W. M. Lee, B. S. Williams, S. Kumar, Q. Hu, and J. L. Reno, Opt. Lett. **35**(7), 910 (2010).
[12]Q. Qin, B. S. Williams, S. Kumar, J. L. Reno, and Q. Hu, Nat. Photonics **3**, 732 (2009).
[13]I. Kundu, P. Dean, A. Valavanic, L. Chen, L. Li, J. E. Cunningham, E. H. Linfield, and A. G. Davies, Opt. Express **22**(13), 16595 (2014).
[14]K. Ohtani, M. Beck, and J. Faist, Appl. Phys. Lett. **104**, 011107 (2014).
[15]J. Faist, *Quantum Cascade Lasers* (Oxford University Press, 2013).
[16]J. Faist, F. Capasso, C. Sirtori, D. L. Sivco, A. L. Hutchinson, and A. Y. Cho, Nature **387**, 777 (1997).
[17]M. Amanti, M. Fischer, G. Scalari, M. Beck, and J. Faist, Nat. Photonics **3**, 586 (2009).
[18]T. Y. Kao, Q. Hu, and J. L. Reno, Opt. Lett. **37**(11), 2070 (2012).
[19]Y. Chassagneux, R. Colombelli, W. Maineoult, S. Barbier, H. E. Beere, D. A. Ritchie, S. P. Khanna, E. H. Linfield, and A. G. Davies, Nature **457**, 174 (2009).
[20]COMSOL Multiphysics Finite Element Analyisis Software, Ver 4.3, RF Module.
[21]M. Amanti, G. Scalari, R. Terazzi, M. Fischer, M. Beck, J. Faist, A. Rudra, P. Gallo, and E. Kapon, New J. Phys. **11**, 125022 (2009).
[22]M. Cui, J. N. Hovenier, Y. Ren, N. Vercruyssen, J. R. Gao, T. Y. Kao, Q. Hu, and J. Reno, Appl. Phys. Lett. **102**, 111113 (2013).
[23]M. Fischer, Ph.D. dissertation, ETH Zurich (2011), p. 19951.